Toward Dynamical Sensor Management for Reactive Wall-following

Avik De and Daniel E. Koditschek

Abstract— **We propose a new paradigm for reactive wall-following by a planar robot taking the form of an actively steered sensor model that augments the robot's motion dynamics. We postulate a foveated sensor capable of delivering third-order infinitesimal (range, tangent, and curvature) data at a point along a wall (modeled as an unknown smooth plane curve) specified by the angle of the ray from the robot's body that first intersects it. We develop feedback policies for the coupled (point or unicycle) sensorimotor system that drive the sensor's foveal angle as a function of the instantaneous infinitesimal data, in accord with the trade-off between a desired standoff and progress-rate as the wall's curvature varies unpredictably in the manner of an unmodeled noise signal. We prove that in any neighborhood within which the third-order infinitesimal data accurately predicts the local "shape" of the wall, neither robot will ever hit it. We empirically demonstrate with comparative physical studies that the new active sensor management strategy yields superior average tracking performance and avoids catastrophic collisions or wall losses relative to the passive sensor variant.**

Fig. 1. Our experimental platform: a RHex variant (a hexapedal legged running platform whose horizontal plane dynamics is well approximated by the unicycle model (9) at modest speeds [16]) equipped with a conventional laser scanner idealized as an infinitesimal sensor, seen here tracking a wall as part of our test suite (cf. Section IV-A).

I. Introduction

The ability to follow the boundary of obstacles in the environment gives a robot the freedom to navigate in a higher dimensional ambient space while keeping the motion control problem at the dimensionality of the boundary itself. There is an extensive literature on "bug"-style algorithms with various sensory enhancements and optimizations which provide guarantees on achieving specific navigation [1], mapping or pursuit-evasion [2] goals with sparse sensory and locomotory capabilities.

In this paper we focus on a kinematic planar robot equipped with an actively steerable infinitesimal[1] sensor. The motivation behind our sensor model is that it is closely related to low-bandwidth sensors such as biological or bio-inspired active antennae/whiskers which sense distance[2] [3], [4], tangent [5], [6] or texture [7], as well as to foveating high-bandwidth sensors such as a laser range scanner or a vision system [8] with shape-from-shading [9] or other attention-localizing [10] capabilities. The active steering ability brings an additional degree of freedom to be controlled. While the classical sensor management literature [11], [12], [13], [14], [15] focuses on optimal (with respect to estimation error or information theoretic considerations) sensor placement, we seek a real-time control strategy for the coupled sensorimotor system (which is assumed to have first-order dynamics, and respecting which the coupling must be specifically prescribed) for successful wall-following.

A. Brief Survey of Prior Literature

The past literature on wall-following robots is vast, however we can immediately distinguish this work from potential-field approaches [17], [18], which need a priori knowledge about the environment, as well as from approaches based on mapping [19], [20], which require more sophisticated sensors than assumed here and need relatively high computational power and memory. We want to restrict attention to the so-called "reactive" or "feedback" [21] paradigm of robot control, where the task is specified as a dynamical relation instead of a prescribed plan. Methods of this genealogy present desirable traits such as faster response time in the presence of disturbances and reduced computational cost, thereby reducing the complexity of the task while expressing a degree of robustness to unstructured environments due to the minimality of its model.

Even among reactive wall-following methods, there is a large literature [22], [23] on methods which successfully prove internal stability with smooth controllers in restrictive environments, with an added layer of discrete switching to circumvent an enumerated set of environmental obstacles. We argue that it is very difficult to make concrete conclusions about the stability or performance of the resulting hybrid system in the presence of unmodeled external perturbations. Our approach instead assumes a very myopic sensor with a

The authors are affiliated with the Electrical and Systems Engineering department, University of Pennsylvania, Philadelphia, PA 19104. Contact: {avik,kod}@seas.upenn.edu

This work was supported by AFOSR MURI FA9550-10-1-0567.

[1]We define "infinitesimal" as a narrow field-of-view sensor which can measure range, tangent and curvature of a smooth curve at one point.

[2]Though, repeated distance measurements in a small neighborhood can be used to approximate tangent, and likewise for curvature.

correspondingly minimal environment model[3]; this simplicity admits a proof of successful wall-following by the robot in an unknown environment.

B. Organization and Contributions of the Paper

The central contributions of this paper are: (a) introduction of a novel active sensing model to the established problem domain resulting in an explicit sensor feedback control law (6) that is empirically shown to dramatically improve performance over a passive sensor implementation (robot experiments are reported in Section IV-A), (b) novel task specification relative to a continuum goal-set as a point-set in a *controlled* moving frame (see Section II), and (c) convergence and tracking guarantees in the (infinitesimal) moving frame (presented as Propositions 1, 2 and 3 in Section II) as well local[4] guarantees of wall avoidance in Propositions 5 and 7 in Section III.

The intuition that a reactive wall-following robot in environments with corners could benefit from a positive (negative) look-ahead at concave (convex) corners motivates the need for a real-time active sensor. In some motivational prior work with an infinitesimal passive sensor for rapid wall-following [25], the authors proved internal stability of the system and had a basin of attraction large enough to reject small external perturbations (corners), but it was necessary to resort to a switching control scheme to handle large deviations from equilibrium. We posit that our proposed active sensing strategy could be directly applied to eliminate the need for any heuristic switching.

While our "local" analysis is still myopic, we are able to provide conditions directly related to the robot state and curvature-like perturbation terms which can provide almost-global guarantees against failure, and which are not considered in typical controller stability analyses [26], [27] in the prior literature from the best of our reading.

Absent an explicit model of the environment we perform the analysis in a moving local frame (a method introduced by Justh et. al. [28]). Using this method, the task-induced symmetry [29] presents itself as a nonzero "drift" term in our dynamical system, so that our goal manifold in world coordinates is just a point in the local frame—a fact that simplifies the analysis greatly. Further, our proposed unicycle controller of Section II-B demonstrates the advantages of a smooth controller that is allowed to set the speed as well as the turning rate. We hypothesize that a large body of existing unicycle control literature that assumes that the system has fixed forward speed [24], [26] could benefit from this insight.

II. Infinitesimal Controller

Model the wall as a simple smooth plane curve of bounded curvature which has the explicit form $b : \mathbb{R}_+ \to \mathcal{Y} \subset \mathbb{R}^2$. Let $\mathrm{D}b$ denote the map to the tangent vector and κ the map to the signed curvature at a point on the curve. We don't require that the curve be unit-speed parameterized, but define $\mathrm{D}b^u$ as the unit tangent, and $\bar{\kappa} = \frac{\kappa}{\|\mathrm{D}b\|}$ the normalized curvature. Define $|\bar{\kappa}|_{\max}$ as the maximum value attained by the $|\bar{\kappa}|$ function.

TABLE I

List of important symbols

Name	First appears	Meaning
b	Section II	Explicit form of wall
β	Proposition 4	Implicit form of wall
$\bar{\kappa}$	Section II	Signed, normalized wall curvature
ρ	Section II	Robot rate of progress
p	Section II	Point robot position (world frame)
q	Section II-A	Point robot position (local frame)
E	Section II-A	Transformation to local frame
φ	Section II-A	Sensor pointing angle
υ	(1)	Sensor steering rate (input)
$\widetilde{u}$	II-A	Point robot velocity (input)
(p, θ)	Section II-B	Unicycle robot configuration (world frame)
r	Section II-B	Unicycle configuration (local frame)
u_1	Section II-B	Unicycle forward speed (input)
u_2	Section II-B	Unicycle steering rate (input)

We assume without loss of generality that the goal is to traverse the curve along the direction $\mathrm{D}b$ while staying on the same side as the normal $J\mathrm{D}b$ (where $J = \left[\begin{smallmatrix} 0 & -1 \\ 1 & 0 \end{smallmatrix}\right]$), and to attempt to maintain a rate of progress $\rho := \|\mathrm{D}b\|\dot{\sigma} \approx 1$.

Additionally, assume that if the robot postion is $p \in \mathbb{R}^2$, and $b(\sigma)$ is the sensed point on the curve (implicitly assumed to be within any sensing range limit), then the infinitesimal sensor measures $\|p - b(\sigma)\|$, $\mathrm{D}b(\sigma)$ and $\bar{\kappa}(\sigma)$.

A. Point Robot

The unitary matrix $E^T = (\mathrm{D}b^u, J\mathrm{D}b^u)$ can be used to change coordinates to and from the local tangent-normal frame, $q = E(p - b(\sigma))$. Additionally, imagine that the point robot has a preferred "direction" oriented along $\mathrm{D}b$ (even though it has no motion constraints as the unicycle does), and note that $\varphi = \angle q$ is the pointing angle of the sensor. In more intuitively illuminating terms, q_2 is the wall stand-off, and $-q_1$ is the look-ahead distance. See Figure 2 for an illustration of the model.

Let both the robot and its sensor be kinematically driven,

$$\dot{p} = E^T \widetilde{u}, \qquad \dot{\varphi} = \upsilon, \tag{1}$$

where we define $\widetilde{u} = (\widetilde{u}_\parallel, \widetilde{u}_\perp)$ in the local frame for convenience. Some trigonometry yields

$$\rho = \widetilde{u}_\parallel + \tfrac{\|q\|^2}{q_2} \upsilon. \tag{2}$$

For convenience, we will substitute ρ for υ in the system equations (1). (As long as $q_2 > 0$ does not cross 0—a condition which is ensured in steady-state by the proof of Proposition 1—we can do this freely.) We examine the consequences of not having control of υ (passive sensor) in Proposition 1.

Using the Frenet-Serret formulae [30], $\dot{E} = -\dot{\sigma}\kappa J E = -\rho\bar{\kappa} J E$, and using (2), we get the simple local kinematics

$$\dot{q} = \widetilde{u} + \rho n, \tag{3}$$

[3] Recent work with sonar [24] introduces a "richer" sensor (reporting a 2D area rather than our ray), but incurs more restrictive assumptions violated by our target operating regime of cluttered corridors and hallways.

[4] We define local in Section III to be a small neighborhood of the robot's position where a second-order approximation of the wall is admissible. We presume that in most non-adversarial settings, such a neighborhood will be considerably larger than that bounded by the sensory horizon.

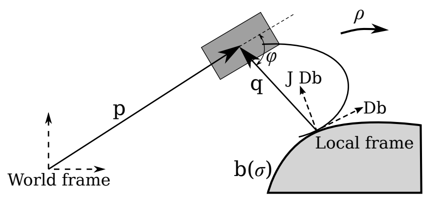

Fig. 2. Our assumed model, with a cartoon depiction of an antenna as the exemplar infinitesimal sensor attached to the (shaded rectangle) mobile robot, and the environment (shaded region lower right).

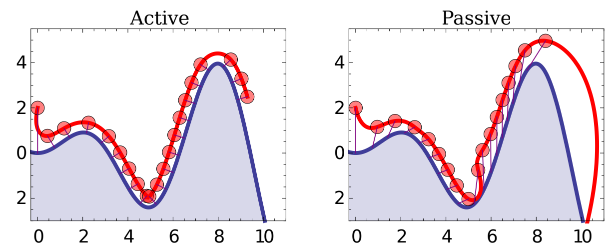

Fig. 3. The trajectory of the simulated point robot, showing tracking failure when the robot is asked to maintain constant rate of progress without active sensing. We choose the curve $b(\sigma) = \left(\sigma, \frac{1}{2}\sigma \sin \sigma\right)$, because it contains curvature spikes reminiscent of corners in the real world.

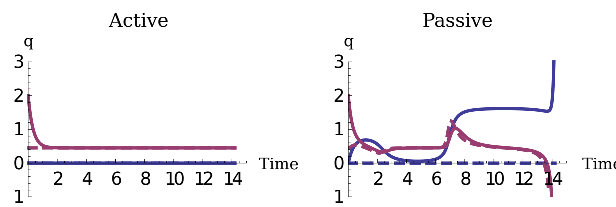

Fig. 4. The evolution of q_1 (in blue) and q_2 (in purple) for the simulated point robot. The dashed lines represent the reference values for each coordinate from (4), $q_1^* = 0$, and $q_2^* = \delta^* + \frac{\bar{\kappa}}{2} q_1^2$. With the exception of q_1 tracking in the passive case (cf. Proposition 1), each other coordinate shows exponential tracking to the goal in the closed-loop system (7)—which explains why the solid lines track the dashed lines so well.

where we define $n := -e_1 - \bar{\kappa} J q$, an unmodeled "noise" vector which includes environmental disturbances through $\bar{\kappa}$, and a constant drift because of the movement of the frame.

Define $\tilde{q}_2 := q_2 - (\delta^* + \frac{\bar{\kappa}}{2} q_1^2)$ as the curvature-corrected tracking error, where our nominal standoff is δ^*.

Proposition 1 (Point robot convergence)**.** *With active sensing, we can assure (a) $\rho = 1$ (desired rate of progress), (b) $\tilde{q}_2 \to 1$, and (c) $q_1 \to 0$, whereas with passive sensing we can only guarantee (a) and (b).*

Proof. Suppose we want to minimize the cost

$$\nu(q) = \frac{1}{2} q_1^2 + \frac{k}{2} \tilde{q}_2^2. \tag{4}$$

We can simply set

$$\widetilde{u} = -\mathrm{D}\nu(q) - \rho n \tag{5}$$

$$\upsilon = \tfrac{q_2}{\|q\|^2} \rho_{\text{desired}} - \widetilde{u}_{\|} \tag{6}$$

to get the closed loop behavior

$$\dot{q} = -\mathrm{D}\nu(q), \qquad \rho = \rho_{\text{desired}}, \tag{7}$$

which ensures $\dot{\nu} = \mathrm{D}\nu \dot{q} = -\|\mathrm{D}\nu\|^2 \leq 0$. In effect, we are using our three control inputs, $\widetilde{u}_{\|}, \widetilde{u}_{\perp}, \upsilon$, to control our three degrees of freedom q_1, q_2, ρ. Section III-A includes a less myopic analysis of this controller.

Without active sensing, in (1) we lose the ability to control ρ through υ, in fact (2) reduces to $\widetilde{u}_{\|} = \rho$. This turns (3) into

$$\dot{q} = \left[\begin{smallmatrix} 0 \\ \widetilde{u}_{\perp} \end{smallmatrix}\right] - \bar{\kappa} J q,$$

showing that q_1 is uncontrollable. Large q_1 results in a detriment to the safety guarantees we can provide under this control by directly jeopardizing the pre-conditions of our proof of local wall-avoidance in Proposition 5. $\square$

B. Unicycle Robot

The point robot design (illustrative simulations in Fig. 3 and 4) extends quite naturally to the unicycle (our horizontal plane model for a quasi-static RHex gait [16]). Define the matrix-valued function $B : \mathrm{SE}(2) \to \mathbb{R}^{3\times 2}$ as

$$B(x, y, \theta) = \left[\begin{smallmatrix} \cos\theta & 0 \\ \sin\theta & 0 \\ 0 & 1 \end{smallmatrix}\right]. \tag{8}$$

We can model the kinematic unicycle with inputs u_1 (forward speed), u_2 (steering rate) and world frame coordinates $(p, \theta) \in \mathrm{SE}(2)$, as $(\dot{p}, \dot{\theta}) = B(p, \theta) u$.

Let $r \in \mathrm{SE}(2)$ be the local frame representation, and $w = \Pi r$ be the projection onto the first two elements. We can follow the same general steps of Section II-A to get the moving-frame system dynamics

$$\dot{r} = B(r) u + \rho n, \qquad \dot{\varphi} = \upsilon, \tag{9}$$

where n is the same as before, and φ is the angle of the pointing direction of the sensor relative to the axis of the unicycle, ie. $\varphi = \tan^{-1}(-E^T w) - \theta$. Similar trigonometry to (2) reveals that

$$\rho = \left[\cos r_3, \tfrac{\|w\|^2}{w_2}\right] u + \tfrac{\|w\|^2}{w_2} \upsilon. \tag{10}$$

As before, we find it easier to treat (u, ρ) as our inputs, where υ is held hostage by the linear constraint equation (10).

Assume that we would like to minimize the cost function $\eta : \mathrm{SE}(2) \to \mathbb{R}_+$,

$$\eta = k_\alpha (1 - \cos \alpha) + \frac{1}{2} r_1^2 + \frac{k}{2} \tilde{r}_2^2, \tag{11}$$

where $\tilde{r}_2 = r_2 - (\delta^* - \frac{\kappa}{2} r_1^2)$, $r_3^* = \tan^{-1}(-k \tilde{r}_2)$, $\alpha = r_3^* - r_3$. The latter two summands are exactly the same as the in (4), and the first term serves the intuitive purpose of steering the unicycle in the direction counter to the offset error, $\tilde{r}_2$.

Define $B(p, \theta)^\times = (-\sin r_3, \cos r_3, 0)$, and note that the non-holonomic motion constraint intuitively results in the system doing a poor job of following the gradient field in the $B^\times$ direction. The effect is more explicit if we change coordinates using the completion of the columns of B. Let

$P := \left[B, B^\times\right]$, $\mathrm{D}\eta = P\left[\begin{smallmatrix} z \\ \zeta \end{smallmatrix}\right]$; then $\lambda = \zeta n^T B^\times$ is the hard-to-cancel component of the gradient in the $B^\times$ direction.

Let $\mu > 0$ be a constant design parameter used to stipulate a "tube" around the $B^\times$-axis, $\mathcal{T}_\mu = \{r : \|z\|^2 \leq \mu,\ \lambda > 0\}$, and let $\mathcal{B}_\mu = \{r \in \mathcal{T}_\mu : \zeta \neq 0\}$. Geometrically, $\mathcal{B}_\mu$ comprises the configurations such that $-\mathrm{D}\eta$ points almost perpendicular to the unicycle's forward axis.

We choose the controller

$$u = B^T(-\mathrm{D}\eta(r) - \rho n), \tag{12}$$

$$\rho = \tfrac{1}{2} - \tfrac{1}{\pi}\tan^{-1}\left(\tfrac{\lambda}{\mu}\right), \tag{13}$$

where $n = -e_1 - \bar{\kappa} J w$. This results in the closed loop dynamics

$$\dot{r} = -Bz + \rho(n^T B^\times)B^\times, \tag{14}$$

$$\dot{\eta} = -\|z\|^2 + \rho\lambda. \tag{15}$$

The unicycle does not offer sufficient control authority to simply "cancel out" the noise to get asymptotic stability in the presence of disturbances as was done for the point robot. however, we make the following claims:

Lemma 2. *Outside the tube $\mathcal{T}_\mu$, we are guaranteed to be reducing the cost: $\dot{\eta}\big|_{r \notin \mathcal{T}_\mu} \leq 0$.*

Proof. Notice in (15) that even though $\dot{\eta}$ is contaminated by a noise term, we can control its magnitude with ρ. We assume that the safety / stability criteria in η are more important than constant rate of progress ($\rho = 1$), and so we use the definition (13), which has the property that $\rho \approx 1$ when $\lambda \leq 0$ and $0 \leq \rho \leq \frac{\mu}{\lambda}$ when $\lambda > 0$.[5] So $\dot{\eta}\big|_{r \notin \mathcal{T}_\mu} \leq -\mu + \mu = 0$. □

The only problem we have to guard against is getting stuck in $\mathcal{B}_\mu$. To that end, we present below a "conservative" analysis that guarantees this. In simulation or experiment, we use more aggressive parameter values, but do not empirically observe any attractors in $\mathcal{B}_\mu$.

Proposition 3 (Conservative unicycle robot convergence)**.** *If $\mu \approx 0$, the system is driven to $\eta = 0$.*

Proof. With this assumption, $\rho > 0$ but $z \approx 0$ in terms of contribution to (14), leading to the simplification $\alpha \approx 0$.

The system dynamics restricted to $\mathcal{B}_\mu$ is

$$\dot{r}\big|_{\mathcal{B}_\mu} = \frac{\rho\lambda}{\zeta} B^\times, \tag{16}$$

where we are allowed to divide by ζ because of the definition of $\mathcal{B}_\mu$. Still restricting everything to $\mathcal{B}_\mu$ some tedious multi-variable calculus shows that $\mathrm{D}(B^T\mathrm{D}\eta)\cdot B^\times = (*, k\gamma^2) \neq 0$. Using this, we get

$$\dot{z}\big|_{\mathcal{B}_\mu} = \mathrm{D}z\big|_{\mathcal{B}_\mu} \cdot \dot{r}\big|_{\mathcal{B}_\mu} = \frac{\rho\lambda}{\zeta}\left(\mathrm{D}(B^T\mathrm{D}\eta)\cdot B^\times\big|_{\mathcal{B}_\mu}\right) \neq 0,$$

which means that we are forced to exit $\mathcal{B}_\mu$. We can conclude that the system is driven to $\eta = 0$, via a trajectory that enters $\mathcal{T}_\mu$ with $\zeta = 0$. □

[5] It is tempting to set $\mu = \|z\|^2$ which would ensure $\dot{\eta} \leq 0$. However, the non-empty kernel of B^T implies that we can have $z = 0$ while $\|\mathrm{D}\eta\| = |\zeta| \neq 0$ (i.e. we are not on the goal set). Further, the restriction of (14) to $z = 0$ yields $\rho = 0,\ \dot{r} = 0$, i.e. the robot would get "stuck".

III. Local Wall-avoidance Guarantees

We claim that our proposed controllers guard against wall penetration in a region (hereforth called a "local" neighborhood) of much larger size than the robot's infinitesimal field of perception. We invoke a global implicit function representation of the curve (unknown to the robot) and use it to prove that the controllers of Section II prevent us penetrating the wall under explicit conditions.

Proposition 4 (Wall implicit function)**.** *There exists a real-valued function β globally defined in a neighborhood of the curve such that*

1) *$\beta \circ b \equiv 0$; it is positive on the side containing the outward normal and negative on the other side,*
2) *$\mathrm{D}\beta\big|_p = \mathbf{n}(p)$, where $p \in \mathcal{Y}$ and $\mathbf{n}(p)$ is the unit outward normal to $\mathcal{Y}$ at p, and*
3) *$E\ \mathrm{D}^2\beta\big|_p E^T = \left[\begin{smallmatrix} -\bar{\kappa}(p) & 0 \\ 0 & 0 \end{smallmatrix}\right]$, where E is the change of basis to local coordinates at p (as in Section II-A).*

Proof. Let $\mathrm{T}_\perp(\mathcal{Y})$ be the normal bundle of $\mathcal{Y}$, and $\mathrm{N}_\varepsilon(\mathcal{Y})$ be an ε-neighborhood of $\mathcal{Y}$ where the Tubular Neighborhood Theorem [31] holds. We conclude that there is a map $\mathrm{T}_\perp(\mathcal{Y}) \to \mathrm{N}_\varepsilon(\mathcal{Y})$ that sends $(p, \varepsilon'\mathbf{n}(p)) \mapsto (p + \varepsilon'\mathbf{n}(p))$ for all $|\varepsilon'| < \varepsilon$ and ε small enough.

Further, since we are on the plane and normals are oriented, we assert that there is a diffeomorphism between $(p, \lambda\mathbf{n}(p)) \in \mathrm{T}_\perp(\mathcal{Y})$ and $(p, \lambda) \in \mathcal{Y} \times (-\epsilon, \epsilon)$, letting us identify $(p, \lambda) \leftrightarrow (p, \lambda\mathbf{n}(p))$.

Composing this last map with the one from the Tubular Neighborhood Theorem, we get the diffeomorphism $f(p, \lambda) = (p + \lambda\mathbf{n}(p))$. Let us define

$$\beta = \pi_2 \circ f^{-1}, \tag{17}$$

where π_2 is the projection to the second element. Now we prove each of the subparts of the Proposition:

1) Observe that $f(p, \lambda)$ for $\lambda > 0$ lies in the same direction as the outward normal.
2) Taking a time derivative of the equation $\beta \circ b = 0$ shows that $\mathrm{D}\beta\big|_{b(\sigma)} \cdot \mathrm{D}b(\sigma) = 0$, so $\mathrm{D}\beta\big|_p$ is parallel to $\mathbf{n}(p)$. To check that it is of unit magnitude,
$$\mathrm{D}\beta\big|_p \cdot \mathbf{n}(p) = \lim_{\lambda \to 0} \frac{\beta(p + \lambda\mathbf{n}(p)) - \beta(p)}{\lambda} = 1$$
3) Note that the hessian is symmetric, and we can find the (1,1) and (1,2) elements by taking derivatives of $\mathrm{D}\beta \cdot \mathrm{D}b^u = 0$ and $\mathrm{D}\beta \cdot (J\mathrm{D}b^u) = 1$. For the (2,2) element, we will do a Taylor expansion of β,
$$\begin{aligned} \lambda &= \beta(p + \lambda\ m) \\ &= \beta(p) + \lambda\mathrm{D}\beta\big|_p m + \tfrac{\lambda^2}{2} m^T\mathrm{D}^2\beta\big|_p m + o(t^2) \end{aligned}$$
$$\implies 0 = \lim_{t \to 0} \frac{t^2\ m^T\mathrm{D}^2\beta\big|_p m}{t^2},$$
and we can conclude that in the direction normal to the curve, $m^T\mathrm{D}^2\beta\big|_p m = 0$. □

Assume the robot is looking at a point $b(\sigma) \in \mathcal{Y}$. We will use a first-order Taylor expansion of $\mathrm{D}\beta$ for the analysis, and

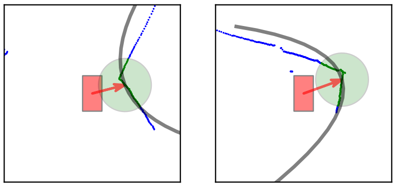

Fig. 5. Implementation of the infinitesimal sensor with a laser scanner: this view from the robot's perspective (moving in the "up" direction) shows the (sub)set of points used to calculate curvature (green disk overlay) as well as the estimated curvature (LS-fitted gray parabola). For this example, $\varepsilon_s = 0.3$.

so we need $\|p - b(\sigma)\|$ to be small. Based on the properties of the curve, fix ε_r such that $\mathcal{Y} \cap \mathrm{N}_{\varepsilon_r}(b(\sigma))$ is approximated well by the Taylor expansion.

A. Point Robot

Proposition 5 (Point robot local safety condition)**.** *If $2k\delta^* > \varepsilon_r$, then under the flow (7), we have*

$$\dot{\beta}\big|_{\mathcal{Y} \cap \mathrm{N}_{\varepsilon_r}(b(\sigma))} > 0,$$

i.e. the robot gets repelled from the wall into the safe region.

Proof. The Taylor expansion at $p \in \mathcal{Y} \cap \mathrm{N}_{\varepsilon_r}(b(\sigma))$ is

$$\begin{aligned}\dot{\beta}\big|_p &= \mathrm{D}\beta\big|_p \cdot \dot{p} \approx \dot{q}^T E \left(\mathrm{D}\beta\big|_{b(\sigma)} + \mathrm{D}^2\beta\big|_{b(\sigma)} E^T q\right) \\ &= \dot{q}^T \left(e_2 - \left[\begin{smallmatrix} \bar{\kappa} & 0 \\ 0 & 0 \end{smallmatrix}\right] q\right) = \dot{q}^T \left[\begin{smallmatrix} -\bar{\kappa} q_1 \\ 1 \end{smallmatrix}\right].\end{aligned}$$

Define $y := \left[\begin{smallmatrix} -\bar{\kappa} q_1 \\ 1 \end{smallmatrix}\right]$. Note that $\mathrm{D}\nu = q_1 e_1 + k\tilde{q}_2 y$. Using (5), (4), and the fact that $q_2 = \frac{\bar{\kappa}}{2} q_1^2$ on $\beta^{-1}(0)$,

$$\dot{\beta}\big|_p = k\delta^* \|y\|^2 + \bar{\kappa} q_1^2. \tag{18}$$

Using the fact that $\max_{\tau \geq 0} \frac{\tau}{1+\tau^2} = \frac{1}{2}$,

$$\left|\frac{\bar{\kappa} q_1^2}{1+\bar{\kappa}^2 q_1^2}\right| = |q_1| \cdot \frac{|\bar{\kappa} q_1|}{1+\bar{\kappa}^2 q_1^2} \leq \frac{|q_1|}{2}.$$

Going back to (18), we get

$$\dot{\beta}\big|_p \geq \|y\|^2 \left(k\delta^* - \frac{|q_1|}{2}\right) \geq 0,$$

by the given condition as long as we are in $\mathrm{N}_{\varepsilon_r}(b(\sigma))$. The condition of being in the ε_r-ball is automatically enforced by the asymptotic stability guarantee of (5).

This result together with the claims in Proposition 1 shows that the active sensing capability is crucial in giving safety and performance guarantees. $\square$

B. Unicycle Robot

Unlike the point robot, it is necessary for the unicycle to allow a buffer region or "collar," $\mathcal{C} \approxeq \mathcal{Y} \times (0, \varepsilon_w]$, of width $0 < \varepsilon_w \ll \delta^*$ in which the controller has time to act. Define $\partial\mathcal{C} := \mathrm{Im}\{b + \varepsilon_w(\mathbf{n} \circ b)\}$, the curve which is the ε_w-extrusion of the wall. We show that if the robot starts from an arbitrary configuration on $\partial\mathcal{C}$, then the control (12) prevents a collision.

If the local frame coordinates of the robot are $r \in \mathrm{SE}(2) \cap (\mathrm{N}_{\varepsilon_r}(0) \times S^1)$, define $y := \left[\begin{smallmatrix} -\bar{\kappa} r_1 \\ 1 \end{smallmatrix}\right]$ and $\chi := \frac{\bar{\kappa}^2 r_1^2}{2\|y\|}$. The following Lemma establishes some technical results necessary for our proof of wall-avoidance in Proposition 7.

Lemma 6. *On the boundary of the collar, $\partial\mathcal{C}$, the closed loop system (14) exhibits*

1) $\dot{\beta}\big|_{\partial\mathcal{C}} \geq -(1+\chi)\|y\|^2$, *and*
2) $\dot{\beta} < 0 \implies \ddot{\beta} \geq 2k\delta^* \|y\|^2 (k_\alpha - |\bar{\kappa}|_{\max})$.

Proof. On $\partial\mathcal{C}$, $r_2 = \frac{\bar{\kappa} r_1^2}{2} + \varepsilon_w$. Assume that k is large enough that $k\delta^* \gg \varepsilon_w$. We get the simplifications (a) $-\mathrm{D}\eta = k\delta^* y$, and (b) $n = Jy + \frac{\bar{\kappa}^2 r_1^2}{2} e_1 = Jy + \chi\|y\| e_1$, where .

1) Just like the particle computation above,
$$\dot{\beta} = y^T \dot{w} \geq \|y\|^2 (k\delta^* (e_u^T y^u)^2 - \rho - \rho\chi).$$
The lower bound to this (in the Lemma statement) is attained when $e_u^T y^u = 0$ and $\rho = 1$.
2) If $\dot{\beta} < 0$, then $|e_u^T y^u|$ is small; let $e_u^T y^u = \xi$ where $k\delta^* \xi^2 \geq 1 + \chi$. Additionally, without loss of generality choose the sign $(y^u)^T J e_u = 1$. Then
$$\dot{\beta} = \|y\|^2 (k\delta^* \xi^2 + \rho\xi + \rho\chi e_u^T e_2). \tag{19}$$
Let $R_\alpha = e^{\alpha J} \in \mathrm{SO}(2)$, and then $e_u = R_\alpha^T e_2$. Taking a derivative, and noting that the closed-loop system (14) sets $\dot{\alpha} = k_\alpha \sin\alpha$ leads to $\dot{e}_u = k_\alpha \sin(\alpha) J e_u$, and $\dot{\xi} = (k_\alpha \sin(\alpha) - \rho\bar{\kappa})$. Note that
$$\begin{aligned}\sin\alpha = e_2^T R_\alpha e_1 &= e_u^T e_1 \approx e_u^T J^T J e_1 \\ &= (y^u)^T J e_1 = \left[1, \bar{\kappa} w_1\right] e_1 = 1,\end{aligned}$$
which means $e_2^T e_u \approx 0$. Lastly,
$$\dot{\|y\|^2} = 2\|y\| y^T \dot{y}^u = 2\|y\| y^T (-\rho\bar{\kappa}(y^u)^T J) = 0.$$
Using these in (19), we get
$$\begin{aligned}\ddot{\beta} &= \|y\|^2 (2k\delta^* \xi + \rho)\dot{\xi} \\ &\geq 2k\delta^* \|y\|^2 (k_\alpha - |\bar{\kappa}|_{\max}).\end{aligned}$$
$\square$

In the following Proposition, we use an infinitesimal condition, $w \in \mathrm{N}_{\varepsilon_r}(0)$—which is under the jurisdiction of the infinitesimal controller's tracking prowess—to give a local guarantee of success.

Proposition 7 (Unicycle robot local safety condition)**.** *If the robot with local coordinates r such that $w(0) \in \mathrm{N}_{\varepsilon_r}(0) \cap \partial\mathcal{C}$ uses a controller where the controller gains are such that*

$$k_\alpha \geq |\bar{\kappa}|_{\max} + \frac{(1 + 2|\bar{\kappa}|_{\max}\varepsilon_r)^2 (1 + |\bar{\kappa}|_{\max}^2 \varepsilon_r^2)}{\varepsilon_w k\delta^*}, \tag{20}$$

then

1) *the maximal "incursion time" that the robot can spend inside $\mathcal{C}$ approaching the wall (with $\dot{\beta} < 0$) is*
$$t_i \leq \frac{1+\chi}{2k\delta^*(k_\alpha - |\bar{\kappa}|_{\max})}, \text{ and}$$
2) *the robot does not reach the wall in this incursion period, i.e.* $\min_{t \leq t_i} \beta(t) = \beta(t_i) > 0$.

Proof. Assuming we start at time $t = 0$ at a distance ε_w from the wall, the latest time t_i by which $\dot{\beta}(t)$ crosses 0 is given by

$$\begin{aligned}0 &= \dot{\beta}(0) + \int_0^{t_i} \ddot{\beta} \\ &\geq t_i \left(2k\delta^* \|y\|^2 (k_\alpha - |\bar{\kappa}|_{\max})\right) - (1+\chi)\|y\|^2,\end{aligned}$$

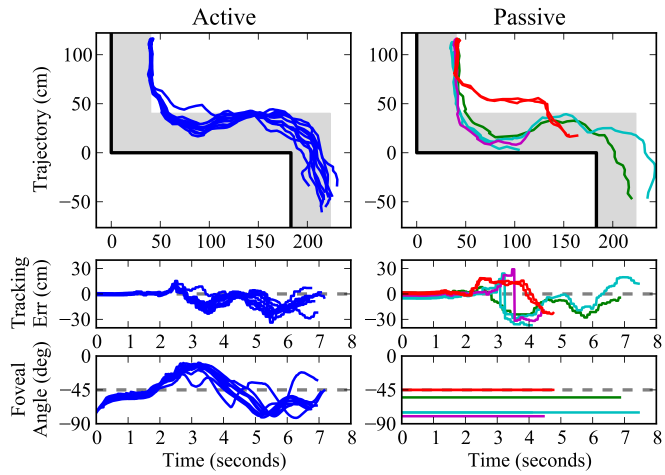

Fig. 6. Ground truth data comparing active and passive sensing strategies in the test environment of Fig. 1. For the passive sensor implementation, we tried a sweep of fixed φ values (bottom right plot). The red trajectories correspond to a $\varphi = -45°$ (forward-looking) configuration, which is adept at concave corners, but fails at the convex one because it turns into the wall too soon. (Recall that our system is memoryless; intuitively the robot must apply a control action as soon as it senses the convex corner, even though it has not approached it yet because of the larger "look-ahead".) The magenta trajectories correspond to a $\varphi = -80°$ (right-looking) configuration which would be capable of navigating the convex corner, but senses the concave corner too late to be able to avoid the next wall segment. The active sensor sweeps a gamut of angles (bottom left), automatically creating for itself a larger (smaller) look-ahead at the concave (convex) corner.

and the first claim follows. The $\mathrm{N}_{\varepsilon_r}(0)$ bound provides $\chi \leq 2|\bar{\kappa}|_{\max}\varepsilon_r$ and $\|y\| \leq 1 + |\bar{\kappa}|^2_{\max}\varepsilon_r^2$. Using our lower bound on $\dot{\beta}$, we can check that to ensure $\beta(t_i) \geq 0$, we need

$$\beta(t_i) = \varepsilon_w + \int_0^{t_i} \dot{\beta} \geq \varepsilon_w - (1+\chi)\|y\|^2 t_i,$$

a sufficient condition for which is exactly (20). □

As a consequence of this Proposition, we can be assured that even if the robot approaches the wall at an arbitrarily bad configuration, the control action manages to steer it away from the wall and avoid failure within the ε_w collar.

IV. Robot Experiments

We use the XRL platform [16] with a Hokuyo UBG-04LX-F01 laser scanner mounted rigidly, such that we scan on the horizontal plane in a 240° arc in front of the robot.

We instantiate our modeled infinitesimal sensor from the laser scanner as in Fig. 5, and choose appropriate controller parameters[6] for all of the following experiments.

A. Comparing Active to Passive Sensing

We set up a test course with the basic building blocks of typical indoor environments, right-angle corners (robot moves from right to left in Fig. 1). We present the tracking performance with ground truth [32] data in Fig. 6.

[6] We use a range of 0.2 - 0.5 meters standoff and our parameter values are chosen aggressively (e.g. $\mu = 0.1$, or ε_s chosen opportunistically to match the "bumpiness" of the wall) relative to the conservative "guaranteed" values in Propositions 3 and 7, albeit with no adverse empirical consequences.

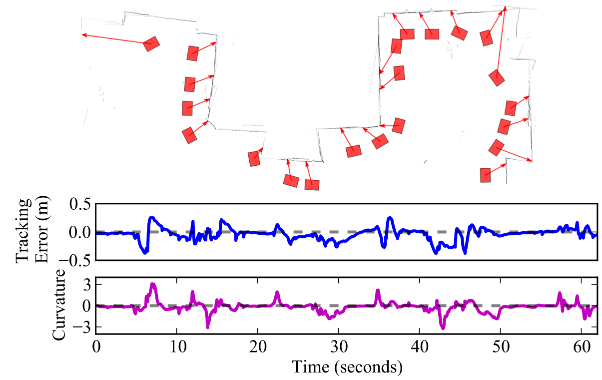

Fig. 7. Application of our controller to an indoor hallway with corners and obstacles. The tracking error displayed is from the robot's perception.

The experiments validate our general intuition that for a reactive behavior, a constant-φ strategy is easily defeated on at least some kind of corner or feature in the environment.

B. Application to Complex Real-world Environments

Even though our model world assumes bounded curvature, the perturbation rejection characteristics of our controller enables us to get good performance in unmodeled and relatively unstructured environments. Because of the lack of a portable ground-truth mechanism, the trajectories in figures in this subsection were generated by manual scan-matching, and are thus suggestive but not exact.

Fig. 7 shows the robot tracking the wall in an indoor hallway with sharp corners and clutter successfully. Note that the measured $\bar{\kappa}$ is what primarily affects tracking error.

Fig. 8 gives anecdotal evidence of some settings where the controller-sensor combination fails, as detailed in the caption.

V. Conclusions and Future Work

We have developed a real-time method for feedback control of a coupled sensorimotor system for two planar kinematic systems. We have supplied some analytical guarantees of controller stability and convergence (Section II), and guarantees against failure (Propositions 5 and 7) as long as the robot stays near the sensed point (Section III).

We have implemented this controller on a RHex robot, and demonstrated (a) that it performs qualitatively better than an equivalent passive-sensor system (Section IV-A), and (b) good tracking capability in unmodeled real-world settings (Section IV-B). We envision that the wall-following capability can augment more complex behaviors, such as landing behavior in autonomous stair-climbing [33].

In this paper we restricted ourselves to a first-order model for robot and sensor, and a future extension to second-order systems seems natural. For the progress-rate goal, this would enable the construction of a point attractor around the reference speed, versus its present manifestation as a linear constraint on the input space in equations (6) and (10).

The speed of the robot in our experiments was limited by invalidity of the unicycle model assumptions at high speeds, resulting in failure to execute the desired control (12). In

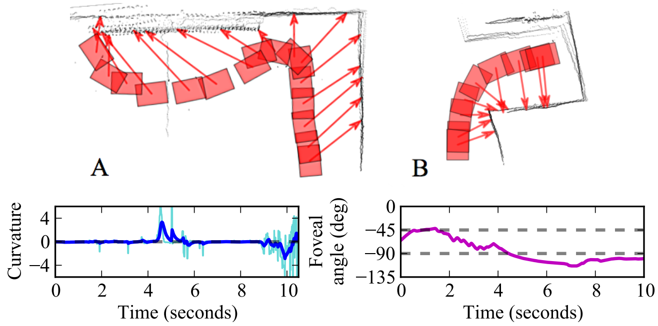

Fig. 8. Examples of environments which could cause failure: **A)** a wall with a grating (on the top edge), and **B)** a small nook in a corridor, the total dimensions of which are comparable to one body length of the robot. The bottom row shows the data corresponding to the likely failure modes in each case: highly noisy (incurred by the high spatial frequence of the grating) raw (cyan) and filtered (blue, Kalman filter output with $\epsilon_s = 0.2$) curvature signals on the left for **A**, and φ with decreasing $|\dot{\varphi}|$ on the right for **B**. The problem in **A** can be attenuated by (a) choosing a larger ε_s, or (b) filtering the raw data. In **B**, the slow traversal speed necessitated by the tight environment precludes sufficiently rapid recovery from the initial convex corner, a consequence of our naively slaving $\dot{\varphi}$ to the robot motion (likely ameliorated, e.g., by a second-order sensor model).

the future we would like to adapt an LLS model [34] for our robot, which could be better suited to control of an even faster wall-following behavior.

Acknowledgments

We thank Dan Guralnik for his insight and help with Proposition 4, and Karl Bayer for initial experimental evidence and programming infrastructure development.

References

[1] J. Ng and T. Bräunl, "Performance comparison of bug navigation algorithms," *Journal of Intelligent & Robotic Systems*, vol. 50, no. 1, pp. 73–84, 2007.

[2] M. Katsev, A. Yershova, B. Tovar, R. Ghrist, and S. LaValle, "Mapping and pursuit-evasion strategies for a simple wall-following robot," *IEEE Transactions on Robotics*, vol. 27, no. 1, pp. 113–128, Feb. 2011.

[3] N. J. Cowan, "Task-level control of rapid wall following in the american cockroach," *Journal of Experimental Biology*, vol. 209, no. 9, pp. 1617–1629, May 2006.

[4] D. Kim and R. Möller, "Passive sensing and active sensing of a biomimetic whisker," in *International Conference on the Simulation and Synthesis of Living Systems. Bloomington: Indiana University Press*, 2006, pp. 127–131.

[5] M. Kaneko, N. Kanayama, and T. Tsuji, "Active antenna for contact sensing," *IEEE Transactions on Robotics and Automation*, vol. 14, no. 2, pp. 278–291, Apr. 1998.

[6] T. Yata, L. Kleeman, and S. Yuta, "Wall following using angle information measured by a single ultrasonic transducer," in *Robotics and Automation, 1998. Proceedings. 1998 IEEE International Conference on*, vol. 2, 1998, pp. 1590–1596.

[7] M. J. Hartmann, "Active sensing capabilities of the rat whisker system," *Autonomous Robots*, vol. 11, no. 3, pp. 249–254, 2001.

[8] D. P. Tsakiris and A. A. Argyros, "Nonholonomic mobile robots equipped with panoramic cameras: Corridor following," *FORTH Institute of Computer Science-Technical Report*, vol. 26, 2000.

[9] R. Zhang, P.-S. Tsai, J. Cryer, and M. Shah, "Shape-from-shading: a survey," *IEEE Transactions on Pattern Analysis and Machine Intelligence*, vol. 21, no. 8, pp. 690–706, Aug. 1999.

[10] H. Yamamoto, Y. Yeshurun, and M. D. Levine, "An active foveated vision system: Attentional mechanisms and scan path covergence measures," *Computer Vision and Image Understanding*, vol. 63, no. 1, pp. 50–65, Jan. 1996.

[11] T. Mukai and M. Ishikawa, "An active sensing method using estimated errors for multisensor fusion systems," *IEEE Transactions on Industrial Electronics*, vol. 43, no. 3, pp. 380–386, 1996.

[12] W. Burgard, D. Fox, and S. Thrun, "Active mobile robot localization," in *In Proceedings of IJCAI-97. IJCAI, Inc*. Morgan Kaufmann, 1997.

[13] L. Mihaylova, T. Lefebvre, H. Bruyninckx, K. Gadeyne, and J. D. Schutter, "Active sensing for robotics - a survey," in *Intl. Conf. On Numerical Methods and Applications*, 2002, pp. 316–324.

[14] C. Kreucher, K. Kastella, and A. O. Hero III, "Sensor management using an active sensing approach," *Signal Processing*, vol. 85, no. 3, pp. 607–624, Mar. 2005.

[15] A. Seekircher, T. Laue, and T. Röfer, "Entropy-based active vision for a humanoid soccer robot," *RoboCup 2010: Robot Soccer World Cup XIV*, pp. 1–12, 2011.

[16] K. C. Galloway, G. C. Haynes, B. D. Ilhan, A. M. Johnson, R. Knopf, G. Lynch, B. Plotnick, M. White, and D. E. Koditschek, "X-RHex: A highly mobile hexapedal robot for sensorimotor tasks," University of Pennsylvania, Tech. Rep., 2010.

[17] S. Charifa and M. Bikdash, "Adaptive boundary-following algorithm guided by artificial potential field for robot navigation," in *IEEE Workshop on Robotic Intelligence in Informationally Structured Space*, 2009, pp. 38–45.

[18] S. Garrido, L. Moreno, D. Blanco, and M. l. Munoz, "Sensor-based global planning for mobile robot navigation," *Robotica*, vol. 25, no. 2, pp. 189–199, Mar. 2007.

[19] S. Fazli and L. Kleeman, "Simultaneous landmark classification, localization and map building for an advanced sonar ring," *Robotica*, vol. 25, no. 03, pp. 283–296, 2007.

[20] S. Thrun and A. Buecken, *Learning Maps for Indoor Mobile Robot Navigation*, ser. Research paper. School of Computer Science, Carnegie Mellon University, 1996, no. v. 96-121.

[21] D. E. Koditschek, "Task encoding: Toward a scientific paradigm for robot planning and control," *Robotics and Autonomous Systems*, vol. 9, no. 12, pp. 5–39, 1992.

[22] Y. Ando and S. Yuta, "Following a wall by an autonomous mobile robot with a sonar-ring," in *IEEE International Conference on Robotics and Automation*, vol. 3, 1995, pp. 2599–2606.

[23] J. M. Toibero, F. Roberti, and R. Carelli, "Stable contour-following control of wheeled mobile robots," *Robotica*, vol. 27, no. 01, p. 1, Apr. 2008.

[24] A. S. Matveev, C. Wang, and A. V. Savkin, "Real-time navigation of mobile robots in problems of border patrolling and avoiding collisions with moving and deforming obstacles," *Robotics and Autonomous Systems*, vol. 60, no. 6, pp. 769–788, June 2012.

[25] A. G. Lamperski, O. Y. Loh, B. L. Kutscher, and N. J. Cowan, "Dynamical wall-following for a wheeled robot using a passive tactile sensor," in *In IEEE Int. Conf. Robot. & Autom*, 2005, pp. 3838–3843.

[26] M. Malisoff, F. Mazenc, and F. Zhang, "Stability and robustness analysis for curve tracking control using input-to-state stability," *IEEE Transactions on Automatic Control*, vol. 57, no. 5, pp. 1320–1326, May 2012.

[27] J. Kim, F. Zhang, and M. Egerstedt, "Curve tracking control for autonomous vehicles with rigidly mounted range sensors," *Journal of Intelligent & Robotic Systems*, vol. 56, no. 1, pp. 177–197, 2009.

[28] E. Justh and P. Krishnaprasad, "Natural frames and interacting particles in three dimensions," in *Decision and Control, 2005 and 2005 European Control Conference. CDC-ECC '05. 44th IEEE Conference on*, dec. 2005, pp. 2841–2846.

[29] V. Kallem, D. E. Chang, and N. J. Cowan, "Task-induced symmetry and reduction in kinematic systems with application to needle steering," in *IEEE/RSJ International Conference on Intelligent Robots and Systems*, 2007, pp. 3302–3308.

[30] R. Millman and G. Parker, *Elements of differential geometry*. Prentice-Hall, 1977.

[31] V. Guillemin and A. Pollack, *Differential Topology*, ser. AMS Chelsea Publishing Series. American Mathematical Society, 2010.

[32] E. Olson, "Apriltag: A robust and flexible multi-purpose fiducial system," University of Michigan, Tech. Rep., May 2010.

[33] A. M. Johnson, M. T. Hale, G. C. Haynes, and D. E. Koditschek, "Autonomous legged hill and stairwell ascent," in *IEEE International Workshop on Safety, Security, & Rescue Robotics, SSRR*, November 2011, pp. 134–142.

[34] R. J. Full and D. E. Koditschek, "Templates and anchors: neuromechanical hypotheses of legged locomotion on land," *Journal of Experimental Biology*, vol. 202, no. 23, pp. 3325–3332, Dec. 1999.